# Resonant Polariton Thermal Transport Along a Vacuum Gap

Sebastian Volz, Masahiro Nomura, and Jose Ordonez-Miranda

Phys. Rev. Applied **18**, L051003 — Published 21 November 2022

DOI: 10.1103/PhysRevApplied.18.L051003

# Resonant Polariton Thermal Transport along a Vacuum Gap

Sebastian Volz,[1,2] Masahiro Nomura,[2] and Jose Ordonez-Miranda[1,2,*]

[1] *LIMMS, CNRS-IIS UMI 2820, The University of Tokyo, Tokyo 153-8505, Japan*
[2] *Institute of Industrial Science, The University of Tokyo, Tokyo 153-8505, Japan*

(Dated: November 1, 2022)

The in-plane thermal conductance of a vacuum gap supporting the propagation of hybridized guided modes along its interfaces with two polar $SiO_2$ materials is quantified and analyzed as a function of the gap distance and temperature. In contrast to the well-known cross-plane thermal conductance, we show that the in-plane one increases with the gap distance up to 1 cm, in which it takes its maxima that increase with temperature. A maximum thermal conductance per unit width of 103 $mWm^{-1}K^{-1}$ is found at 500 K, which is more than 6 (3) orders of magnitude higher than the corresponding one found in the near-field (far-field) regime. This top polariton thermal conductance along the cavity is pretty much equal to the radiative one predicted by Planck's law and therefore it could be useful to amplify or evacuate heat currents along macroscale gaps.

Surface phonon-polaritons (SPhPs) are electromagnetic surface modes generated by the coupling of infrared photons with optical phonons at the interface of polar materials [1–3]. These surface excitations are able to propagate a distance much longer than the typical mean free paths of phonons and electrons, which makes of them powerful energy carriers [4–9]. In thermal radiation across a vacuum gap, for instance, the evanescent coupling of SPhPs inside the gap can enhance the heat transport several orders of magnitude over the blackbody limit [10–15]. This remarkable enhancement appears in the near-field regime and has a wide variety of applications in thermophotovoltaics [16, 17], thermal computing [18] and photonics[19–21].

While the near-field radiation inside a gap is driven by the cross-plane propagation and coupling of evanescent SPhPs, their in-plane propagation can also be exploited to carry heat along surfaces, via propagative modes [4, 5, 22, 23]. Previous theoretical [4, 5] and experimental [24, 25] works revealed that the SPhP contribution to the in-plane heat flux along ultra-thin polar films can actually compete with the their phonon counterparts. This high SPhP contribution arises from the evanescent coupling between the SPhPs propagating along the two nanofilm surfaces, distances longer than the corresponding cross-plane ones outside of the nanofilm [5]. The SPhP coupling shows up not only in single nanofilms, but also in microscale structures, as is the case of a $10-\mu$m-thick silicon layer sandwiched by two $SiO_2$ nanofilms that was recently studied [26]. As a result of the strong coupling of SPhPs propagating along its two $SiO_2$ nanofilms, this $SiO_2/Si/SiO_2$ structure can efficiently enhances the in-plane SPhP heat transport to values ten times higher than the corresponding one of a single $SiO_2$ nanofilm. Taking into account that silicon is a non-absorbing material within a wide range of infrared frequencies relevant for the propagation of SPhPs [27], the coupling of these energy carriers via a vacuum gap is also expected to generate a significant heat current along its interfaces. Furthermore, as the number of SPhP modes increases with the gap distance [1, 26, 28], their thermal activation and combined contribution to this heat current along a microgap could even be comparable to the Planck's limit of thermal radiation, but it is not studied yet, till now.

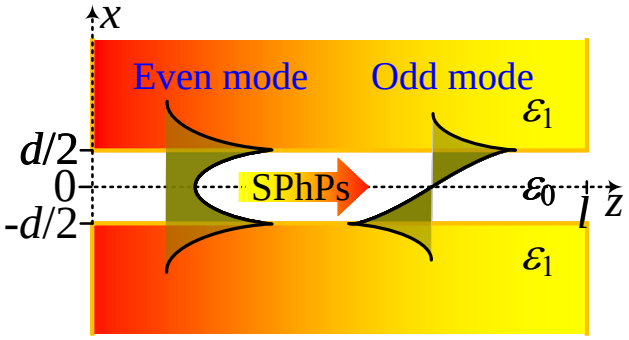


FIG. 1: Scheme of a vacuum gap between two identical semi-infinite polar materials of relative permittivity $\varepsilon_1$. The gap supports the propagation of HGMs via symmetric (even) and antisymmetric (odd) modes.

The purpose of this letter is to theoretically demonstrate the resonant behavior of the in-plane thermal conductance of a vacuum gap, as a function of its distance $d$. In contrast to the well-known cross-plane thermal conductance, it is shown that the in-plane one exhibits its lowest values as $d \to 0$ and its highest one at about $d = 1$ cm. This thermal resonance occurs due to the thermal activation of hundreds of hybridized guided modes (HGMs), resulting from the interaction of SPhP modes with standing waves propagating outside and inside the cavity, respectively. Unlike the single mode supporting the SPhP heat transport along a nanofilm [22], these HGMs maximize their energy density and coupling for a macroscale cavity.

Let us consider a gap supporting the propagation of HGMs along its interfaces with two semi-infinite and identical polar materials, as shown in Fig. 1. These materials have a relative permittivity $\varepsilon_1$ and are separated by a gap of permittivity $\varepsilon_0$ and distance $d$. Assuming

that the surface $z = 0$ of both polar materials is uniformly heated up with a thermal source, the heat propagates along the $z$ axis mainly and the in-plane thermal conductance $G$ of the gap due to HGMs is given by [22]

$$\frac{G}{a} = \frac{1}{2\pi^2}\int \hbar\omega \mathrm{Re}(\beta)\tau(\omega)\frac{\partial f}{\partial T}d\omega, \tag{1}$$

where $a$ is the system width (dimension perpendicular to the xz plane), $\hbar$ is the Planck's constant divided by $2\pi$, $\mathrm{Re}(\beta)$ is the real part of the in-plane HGM wave vector $\beta$, $f = [\exp(\hbar\omega/k_BT) - 1]^{-1}$ is the Bose-Einstein distribution function, $T$ is the average temperature, $k_B$ is the Stefan-Boltzmann constant, $\omega$ is the spectral frequency, and $\tau$ is the transmission probability given by

$$\tau = \frac{\pi}{2\lambda}\left(1 - \frac{4\psi(0)}{\pi\lambda}\right), \tag{2}$$

where $\lambda = l/\Lambda$, $\Lambda = [2\mathrm{Im}(\beta)]^{-1}$ is the HGM in-plane propagation length and $\psi(\xi) = E_5(\xi) - E_5(\lambda - \xi)$, being $E_n(x) = \int_0^{\pi/2}\cos^{n-2}(\theta)e^{-x/\cos(\theta)}d\theta$. Equation (2) thus establishes that the transmission of HGMs along the length $l$ is determined by $\lambda$. In the diffusive regime ($\lambda = l/\Lambda \gg 1$), the ratio $\psi(0)/\lambda \to 0$ and $\tau \approx 0$, while in the ballistic limit ($\lambda \ll 1$), $1 - 4\psi(0)/\pi\lambda \to 2\lambda/\pi$ and $\tau \approx 1$. The HGM heat transport is hence enhanced along a system with a length $l$ smaller than the HGM propagation length ($l \ll \Lambda$), as indicated by Eq. (1). In any case, according to Eqs. (1) and (2), the HGM thermal conductance depends on the material properties through the product $\mathrm{Re}(\beta)\tau(2l\mathrm{Im}(\beta))$ driven by the HGM wavevector $\beta(\omega)$, which is given by the dispersion relation of HGMs propagating along the vacuum gap shown in Fig. 1. As $G$ increases with this product, the optimal material configuration to maximize the HGM heat transport is given by a large wave vector $\mathrm{Re}(\beta)$ and a long propagation length (small $\mathrm{Im}(\beta)$). After solving the Maxwell equations under proper boundary conditions for the transverse magnetic polarization required for the existence of HGMs[4], the following dispersion relations are obtained[1, 28, 29]

$$\varepsilon_0 p_1 + \varepsilon_1 p_0 \tanh(p_0 d/2) = 0, \tag{3a}$$

$$\varepsilon_1 p_0 + \varepsilon_0 p_1 \tanh(p_0 d/2) = 0, \tag{3b}$$

where the cross-plane wavevectors $p_n$ are given by $p_n^2 = \beta^2 - \varepsilon_n k_0^2$, with $k_0 = \omega/c$ and $c$ being the wavevector and speed of light in vacuum, respectively. Equations (3a) and (3b) represent the symmetric (even) and antisymmetric (odd) HGM modes with respect to the magnetic field[29]. For a vacuum cavity ($\varepsilon_0 = 1$) in between two lossless materials ($\mathrm{Im}(\varepsilon_1) = 0$), as is the case of silicon ($\varepsilon_1 = 11.7$) [27], the solutions of Eqs. (3a) and (3b) do not correspond to confined waves and hence the cavity is unable to transport HGM energy. The existence ($\mathrm{Re}(p_n) > 0$) and propagation ($\Lambda > 0$) of HGMs can only be determined for lossy (absorbing) materials ($\mathrm{Im}(\varepsilon_1) > 0$), as is the case of a wide variety of polar dielectrics (i. e. $SiO_2$, SiC, SiN, hBN) [30]. In the "far-field" limit ($|p_0|\, d \gg 2$ or $d \to \infty$), the HGMs propagating along the surfaces $x = \pm d/2$ decouple, $\tanh(p_0 d/2) \to 1$ and Eqs. (3a) and (3b) reduce to the dispersion relation of HGMs propagating along a single interface (SI) $\varepsilon_0 p_1 + \varepsilon_1 p_0 = 0$ [28], which yields

$$\beta = k_0\sqrt{\frac{\varepsilon_0\varepsilon_1}{\varepsilon_0 + \varepsilon_1}}. \tag{4}$$

The HGM wavevector and hence the HGM thermal conductance $G$ of an infinitely thick cavity ($d \to \infty$) become independent of the gap distance. As HGMs propagate along both decoupled interfaces, for this thick cavity $G$ is determined combining Eqs. (1) and (4), and multiplying Eq. (1) by two. On the other hand, in the "near-field" limit ($|p_0|\, d \ll 2$), the odd mode does not support the propagation of HGMs ($\Lambda > 0$), while the even one split into the following two branches (solutions)

$$\beta \approx p_0 \approx p_1 \approx -\frac{2}{d}\frac{\varepsilon_0}{\varepsilon_1}, \tag{5a}$$

$$\frac{\beta}{k_0} \approx \sqrt{\varepsilon_1};\ \frac{p_0}{k_0} \approx \sqrt{\varepsilon_1 - \varepsilon_0};\ \frac{p_1}{k_0} = \frac{2}{d}\left(1 - \frac{\varepsilon_1}{\varepsilon_0}\right)\varepsilon_1 k_0. \tag{5b}$$

Given that in this "near-field" limit, the gap distance $d \to 0$, the branch 1 in Eq. 5(a) is characterized by a large wavevector $\mathrm{Re}(\beta) \propto d^{-1}$ and a small propagation length $\Lambda \propto d$ of HGMs propagating with frequencies satisfying the condition $\mathrm{Re}(\varepsilon_1(\omega)) < 0$. This latter feature results from the strong energy absorption by the polar materials, while the former one is related to the strong coupling of the HGMs propagating along the surfaces $x = \pm d/2$, as shown in the supplementary material (SM) through the analysis of the Poynting vector [29]. According to Eq. (2), the product $\mathrm{Re}(\beta)\tau$ and hence the contribution of the branch 1 to $G$ become independent of $d$. This result also applies for branch 2 in Eq. (5b), which indicates that the HGM thermal conductance in the "near-field" limit is independent of the gap distance, as is the case in the "far-field" regime. The HGM thermal conductance $G(d)$ thus takes two asymptotic values for $d \to 0$ and $d \to \infty$, in which the HGM propagation exhibits strong absorption (small $\Lambda$) and weak coupling (small $\mathrm{Re}(\beta)$), respectively. As none of these two conditions represent the optimal configuration (weak absorption and strong coupling) for maximizing the HGM thermal conductance, the maximum value of $G$ is expected to appear at an intermediate gap distance, as shown below. For a finite $d$ value, both HGM modes in Eqs. (3a) and (3b) have, in general, a infinite number of branches, as $\tanh(p_0 d/2) = \tanh(i\pi n + p_0 d/2)$, for $n = 0, 1, 2, ....$ Taking into account that $\tanh(x + iy) = [\tanh(x) + i\tan(y)]\,/\,[1 + i\tanh(x)\tan(y)] = 1$ for $\tanh(x) = 1$, which is well satisfied for $x > 2$, one of these solutions of both the even and odd modes is given by

the "far-field" mode (Eq. (4)) that shows up for a thick enough gap determined by the condition $\mathrm{Re}(p_0)d > 4$. According to Eq. (4), this inequality is fulfilled for frequencies, such that $J(\omega) > 0$, where

$$J = \frac{(\varepsilon_0 k_0 d)^2}{2^5}\left[|\varepsilon_0+\varepsilon_1| - \mathrm{Re}(\varepsilon_0+\varepsilon_1)\right] - |\varepsilon_0+\varepsilon_1|^2 . \quad (6)$$

In absence of absorption ($\mathrm{Im}(\varepsilon_1) = 0$), Eq. (6) indicates that the persistent "far-field" mode appears for frequencies fulfilling the condition $\mathrm{Re}(\varepsilon_1) < -\varepsilon_0$. In presence of absorption ($\mathrm{Im}(\varepsilon_1) > 0$), this mode appears for frequencies inside and outside the corresponding frequency interval obtained in absence of absorption.

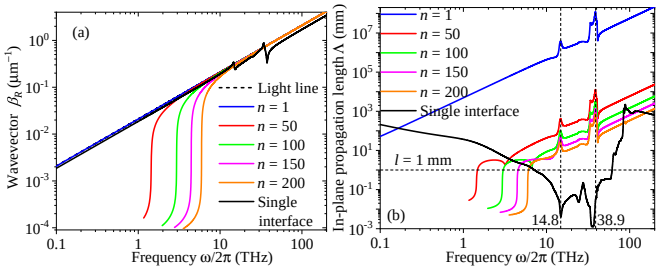


FIG. 2: Spectra of the (a) dispersion relation and (b) in-plane propagation length of HGMs propagating along a 1 cm-surrounded by $SiO_2$, in comparison with the corresponding ones (black lines) obtained for a single interface ($d \to \infty$). Calculations were done for 5 representative branches of the first 200 ones of the symmetric mode.

The HGM propagation parameters and thermal conductance along a vacuum gap ($\varepsilon_0 = 1$) in between two $SiO_2$ materials are now numerically analyzed in comparison with their corresponding counterparts obtained for an infinite gap distance ($d \to \infty$). Calculations are done with the experimental data of the complex and spectral $SiO_2$ permittivity reported in the literature [5] and plotted in the SM [29]. The dispersion relation $\beta_R = \mathrm{Re}(\beta)$ and in-plane propagation length $\Lambda$ of HGMs propagating along a 1-cm-thick vacuum cavity are respectively shown in Figs. 3(a) and 3(b), for 5 representative branches of the first 200 ones of the symmetric mode (Eq. (3a)). Note that $\beta_R$ increases with frequency, such that its first branch ($n = 1$) is pretty much superposed with the light line $k_0 = \omega/c$. Higher-order branches also exhibit this photon-like nature at high enough frequency but reduce the value and span of the wavevector at low frequency. Furthermore, the existence of hundreds of branches with $\beta_R$ values generally higher than those of the SI, for a relevant range of frequencies (see Fig. 4), indicates that the cavity is a better polariton thermal conductor than a SI, as established by Eq. (1). This is confirmed by Fig. 2(b), which shows that the propagation length of HGMs propagating along the cavity is generally greater than that along a SI (black line) and its maxima show up at frequencies (14.8 and 38.9 THz) where the SI propagation length exhibits its minima. This extreme values are induced by the dips of the real part of the permittivity of $SiO_2$, as shown in Fig. S3 of the SM [29]. More importantly, as $\Lambda$ is generally greater than the considered cavity length $l = 1$ mm, HGMs can travel along the whole cavity, which yields a transmission probability $\tau \approx 1$, as determined by Eq. (2). In contrast to the SI, the cavity thus allows to optimize and multiply (several branches) the two parameters $\beta_R$ and $\tau$ enhancing the HGM heat transport along its surfaces.

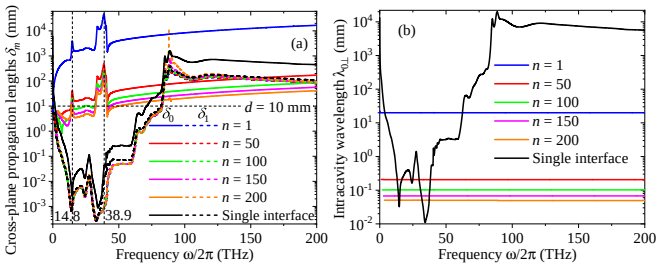


FIG. 3: Spectra of the cross-plane (a) propagation lengths and (b) wavelength of HGMs propagating along a 1-cm-thick gap surrounded by $SiO_2$, in comparison with the corresponding ones (black lines) found for an infinitely thick cavity ($d \to \infty$).

Figure 3(a) shows the frequency dependence of the cross-plane propagation length $\delta_m = [2\mathrm{Re}(p_m)]^{-1}$ inside ($m = 0$) and outside ($m = 1$) the cavity, for 5 representative branches of the first 200 of the symmetric mode. $\delta_m$ drives the exponential decay of the Poynting vector in the cross-plane direction, as established by Eqs. (8) and (9) of the SM. Note that $\delta_0$ reduces as the branch order increases, while $\delta_1$ remains invariant. Since $\delta_0$ is generally greater than the considered cavity distance $d = 1$ cm, in particular for the first branch ($n = 1$), the HGMs propagating alone the two cavity interfaces are strongly coupled. This coupling indicates that the HGM thermal conductance in Eq. (1) represents the contribution of all HGM modes propagating not only along the interfaces, but also inside the cavity. According to Fig. 2(b), this coupling allows HGMs to propagate in-plane distances much longer than those in absence of it (SI case), with a intracavity cross-plane wavelength $\lambda_{0\perp} = 2\pi\,[\mathrm{Im}(p_0)]^{-1}$ independent of frequency, as shown in Fig. 3(b). Shorter wavelengths are obtained for higher-order branches, such that $d = n\lambda_{0\perp}$, for $n = 1, 2, 3, ....$ This latter condition maximizes the HGM Poynting vector along the cavity surfaces $x = \pm d/2$, as demonstrated in the SM[29], and is analogous to the standing waves pattern of a guitar string. This maximization of the electromagnetic energy density of HGMs is directly correlated to the one of their thermal conductance determined by Eq. (1), since they exhibit relatively long in-plane propagation lengths

(transmission $\tau \approx 1$) without a significant reduction of their in-plane wavevector (see Fig. 2). Standing modes of HGMs are thus expected to optimize their heat transport along the cavity. These cavity modes obtained for a cavity distance $d = 1$ cm are also present for other cavity distances, but not for all frequencies and branches, which indicates that the maximum HGM thermal conductance could be obtained for $d = 1$ cm, as confirmed below.

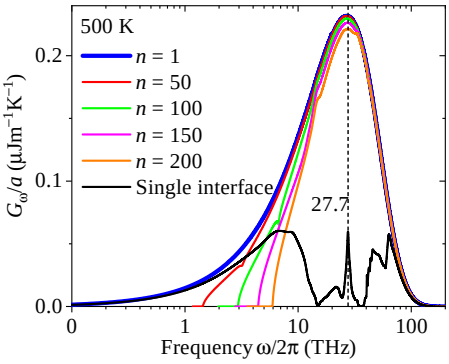


FIG. 4: Spectrum of the HGM thermal conductance for a 1-cm-thick gap surrounded by $SiO_2$, in comparison with the corresponding one (black line) got for a thick gap ($d \to \infty$). Calculations were done for $T = 500$ K.

The contribution of 5 representative branches of the symmetric mode to the spectrum $G_\omega/a$ of the HGM thermal conductance per unit width ($G = \int G_\omega d\omega$ in Eq. (1)) is shown in Fig. 4. The maxima of $G_\omega$ at 27.7 THz indicate that the major contribution to the HGM thermal conductance arises from the vicinity of this frequency that maximize both $\beta_R$ and $\Lambda$, in presence of the high-frequency attenuation of the Bose-Einstein distribution function $f$. Note that the contribution of the branches predicted for a gap distance $d = 1$ cm, are much higher than the corresponding one obtained for an infinitely thick cavity ($d \to \infty$) characterized by two (uncoupled) single interfaces. The 1-cm-thick cavity is therefore able to support the transport of more HGM thermal energy than this latter one, and actually more than a cavity of any other thickness, as shown in Fig. 5(a). For the sake of accuracy, calculations for the 1-cm-thick cavity were done for the first 800 branches with a significant contribution ($G/a > 0.1$ μWm$^{-1}$K$^{-1}$) for each mode (even and odd). Other cavity thicknesses involve a smaller number of branches and not all of them are cavity modes ($d = n\lambda_{0\perp}$) with a significant contribution, which hence yield a lower HGM thermal conductance. Note that the contribution of the even mode is generally higher than that of the odd one, such that their odd/even ratio $\rho$ (green line) increases with the gap distance until reaching the unity for an infinitely thick gap. For nanogaps, on the other hand, $\rho$ goes to zero due to the vanishing contribution of the odd mode, as is the case of nanofilms as well [5]. By contrast, the contributions of both the even and odd modes reach their maxima for a 1-cm-thick cavity with $\rho = 0.85$. The maximum of the total (even+odd) thermal conductance ($G/a = 103$ mWm$^{-1}$K$^{-1}$) is more than 3 orders of magnitude higher than the corresponding one ($G/a = 0.035$ mWm$^{-1}$K$^{-1}$) obtained for a thick cavity ($d \to \infty$) at 500 K. Higher or lower temperatures respectively yield larger or smaller HGM thermal conductances, as shown in Fig. 5(b). For the three considered temperatures, the maxima of $G/a$ appears for a gap distance about $d = 1$ cm and their values are pretty much the same than the corresponding ones that could be obtained by pure radiation, if the cavity surfaces $z = 0; l$ would be excited by a temperature difference $\delta T$, as detailed in the SM [29]. These comparable values indicate that HGMs can be as good as thermal photons to transport heat along a cavity and therefore they could be used to amplify heat currents along macroscale gaps. The sizable gap distance ($d = 1$ cm) along with the relatively high maxima of the HGM thermal conductance are expected to facilitate its observation and application.

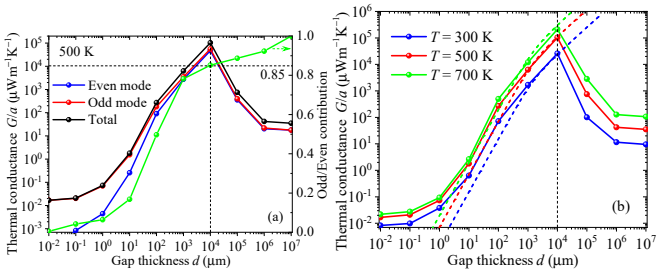


FIG. 5: HGM thermal conductance per unit width of a vacuum gap, as a function of its distance. (a) Contribution of the even and odd modes at 500 K and (b) the total values for three representative temperatures. The green line in (a) stands for the ratio between the odd and even mode contributions, while the dashed lines in (b) represent the predictions of Planck's theory [31], as detailed in the SM [29]. Calculations were done by summing up the contributions of the first 800 branches of each of the even and odd modes, for $a = l = 1$ mm and $\delta T = 10$ K.

Even though the resonant polariton thermal transport reported in this Letter was obtained for a 1-cm-thick cavity surrounded with parallel plates and this parallelism is not difficult to establish for a macroscale cavity, we anticipate that slight deviations from this configuration could lead to other effects. For instance, the lack of alignment between the plates could give rise to focusing or defocusing of HGMs, as reported for conical and wedge structures [32]. Furthermore, the replacement of the flat cavity with a cylindrical one could be used to tailor the resonant energy transport of HGMs.

In summary, the resonant behavior of the in-plane thermal conductance of a vacuum gap supporting the propagation of hybridized guided modes has been studied

as a function of the gap distance. For a 1-cm-thick gap and temperature of 500 K, a maximum thermal conductance per unit width of 103 $\mathrm{mWm^{-1}K^{-1}}$ has been found, which is more than 6 (3) orders of magnitude higher than the corresponding one found in the near-field (far-field) regime. This resonance is generated by the thermal excitation of hundreds of cavity modes that maximize the energy density and coupling of polaritons propagating along the gap interfaces. Furthermore, it has been shown that hybridized guided modes are powerful energy carriers able to transport heat along the cavity as much as thermal photons and therefore they could be useful to enhance or evacuate heat currents along macroscale gaps.

This work was supported by the CREST Japan Science and Technology Agency, grants n° JPMJCR19Q3 and JPMJCR19I1, and the French project ANR-19-CE09-0005 "EPolariton".

* jose.ordonez@cnrs.fr


[1] V. M. Agranovich, *Surface Polaritons* (Elsevier, Amsterdam, 2012).

[2] J. Ordonez-Miranda, L. Tranchant, S. Gluchko, and S. Volz, Energy transport of surface phonon polaritons propagating along a chain of spheroidal nanoparticles, Phys. Rev. B **92**, 115409 (2015).

[3] J. Ordonez-Miranda, L. Tranchant, K. Joulain, Y. Ezzahri, J. Drevillon, and S. Volz, Thermal energy transport in a surface phonon-polariton crystal, Phys. Rev. B **93**, 035428 (2016).

[4] D.-Z. A. Chen, A. Narayanaswamy, and G. Chen, Surface phonon-polariton mediated thermal conductivity enhancement of amorphous thin films, Phys. Rev. B **72**, 155435 (2005).

[5] J. Ordonez-Miranda, L. Tranchant, T. Tokunaga, B. Kim, B. Palpant, Y. Chalopin, T. Antoni, and S. Volz, Anomalous thermal conductivity by surface phonon-polaritons of polar nano thin films due to their asymmetric surrounding media, J. Appl. Phys. **113**, 084311 (2013).

[6] F. Yang, J. R. Sambles, and G. W. Bradberry, Long-range surface modes supported by thin films, Phys. Rev. B **44**, 5855 (1991).

[7] D. Z. A. Chen and G. Chen, Measurement of silicon dioxide surface phonon-polariton propagation length by attenuated total reflection, Appl. Phys. Lett. **91**, 121906 (2007).

[8] J. Ordonez-Miranda, L. Tranchant, T. Antoni, Y. Chalopin, and S. Volz, Thermal conductivity of nano-layered systems due to surface phonon-polaritons, J. Appl. Phys. **115**, 054311 (2014).

[9] S. Gluchko, B. Palpant, S. Volz, R. Braive, and T. Antoni, Thermal excitation of broadband and long-range surface waves on sio2 submicron films, Appl. Phys. Lett. **110**, 263108 (2017).

[10] E. Rousseau, A. Siria, G. Jourdan, S. Volz, F. Comin, J. Chevrier, and J.-J. Greffet, Radiative heat transfer at the nanoscale (2009).

[11] B. Song, D. Thompson, A. Fiorino, Y. Ganjeh, P. Reddy, and E. Meyhofer, Radiative heat conductances between dielectric and metallic parallel plates with nanoscale gaps (2016).

[12] A. Kittel, W. Müller-Hirsch, J. Parisi, S.-A. Biehs, D. Reddig, and M. Holthaus, Near-field heat transfer in a scanning thermal microscope, Phys. Rev. Lett. **95**, 224301 (2005).

[13] V. Fernández-Hurtado, F. J. García-Vidal, S. Fan, and J. C. Cuevas, Enhancing near-field radiative heat transfer with si-based metasurfaces, Phys. Rev. Lett. **118**, 203901 (2017).

[14] M. Ghashami, H. Geng, T. Kim, N. Iacopino, S. K. Cho, and K. Park, Precision measurement of phonon-polaritonic near-field energy transfer between macroscale planar structures under large thermal gradients, Phys. Rev. Lett. **120**, 175901 (2018).

[15] R. S. Ottens, V. Quetschke, S. Wise, A. A. Alemi, R. Lundock, G. Mueller, D. H. Reitze, D. B. Tanner, and B. F. Whiting, Near-field radiative heat transfer between macroscopic planar surfaces, Phys. Rev. Lett. **107**, 014301 (2011).

[16] A. Fiorino, L. Xu, D. Thompson, R. Mittapally, P. Reddy, and E. Meyhofer, Nanogap near-field thermophotovoltaics (2018).

[17] C. Lucchesi, D. Cakiroglu, J.-P. Perez, T. Taliercio, E. Tournie, P.-O. Chapuis, and R. Vaillon, Near-field thermophotovoltaic conversion with high electrical power density and cell efficiency above 14% (2021).

[18] P. Ben-Abdallah and S.-A. Biehs, Near-field thermal transistor, Phys. Rev. Lett. **112**, 044301 (2014).

[19] A. W. Rodriguez, M. T. H. Reid, J. Varela, J. D. Joannopoulos, F. Capasso, and S. G. Johnson, Anomalous near-field heat transfer between a cylinder and a perforated surface, Phys. Rev. Lett. **110**, 014301 (2013).

[20] S.-A. Biehs, E. Rousseau, and J.-J. Greffet, Mesoscopic description of radiative heat transfer at the nanoscale, Phys. Rev. Lett. **105**, 234301 (2010).

[21] M. Lim, J. Song, S. S. Lee, and B. J. Lee, Tailoring near-field thermal radiation between metallo-dielectric multilayers using coupled surface plasmon polaritons, Nat Commun. **9**, 4302 (2018).

[22] Y. Guo, S. Tachikawa, S. Volz, M. Nomura, and J. Ordonez-Miranda, Quantum of thermal conductance of nanofilms due to surface-phonon polaritons, Phys. Rev. B **104**, L201407 (2021).

[23] J. Ordonez-Miranda, L. Tranchant, B. Kim, Y. Chalopin, T. Antoni, and S. Volz, Quantized thermal conductance of nanowires at room temperature due to zenneck surface-phonon polaritons, Phys. Rev. Lett. **112**, 055901 (2014).

[24] L. Tranchant, S. Hamamura, J. Ordonez-Miranda, T. Yabuki, A. Vega-Flick, F. Cervantes-Alvarez, J. J. Alvarado-Gil, S. Volz, and K. Miyazaki, Two-dimensional phonon polariton heat transport, Nano Lett. **19**, 6924–6930 (2019).

[25] Y. Wu, J. Ordonez-Miranda, S. Gluchko, R. Anufriev, D. D. S. Meneses, L. D. Campo, S. Volz, and M. Nomura, Enhanced thermal conduction by surface phonon-polaritons, Sci. Adv. **6**, eabb4461 (2020).

[26] S. Tachikawa, J. Ordonez-Miranda, Y. Wu, L. Jalabert, R. Anufriev, S. Volz, and M. Nomura, High surface phonon-polariton in-plane thermal conductance along coupled films, Nanomaterials **10**, 1383 (2020).

[27] W. C. Dunlap and R. L. Watters, Direct measurement of

the dielectric constants of silicon and germanium, Phys. Rev. **92**, 1396 (1953).

[28] C. Yeh and S. F. I., *The Essence of Dielectric Waveguides* (Springer, New York, 2008).

[29] S. the Supplemental Material at xyz, for the detailed derivation of the dispersion relation and poynting vector of sphps, as well as the intracavity thermal radiation predicted by planck's law, .

[30] E. D. Palik, *Handbook of Optical Constants of Solids* (Academic Press, Orlando, Florida, 1985).

[31] M. F. Modest, *Radiative Heat Transfer* (Elsevier Science, California, 2003).

[32] S. Gluchko, J. Ordonez-Miranda, L.Tranchant, T. Antoni, and S. Volz, Focusing of surface phonon-polaritons along conical and wedge polar nanostructures, J. Appl. Phys. **118**, 064301 (2015).